Available online at www.sciencedirect.com
ScienceDirect
Journal of Organometallic Chemistry 692 (2007) 3796–3803
Journal of Organometallic Chemistry
www.elsevier.com/locate/jorganchem

Hydride abstraction of methylamine with $Cu^+(^1S)$ in the gas phase: A density functional theory study

Xiaoqing Lu, Wenyue Guo *, Lianming Zhao, Xiangfeng Chen, Qingtao Fu, Yan Ma

College of Physics Science and Technology, China University of Petroleum, Dongying, Shandong 257061, PR China

Received 6 April 2007; received in revised form 6 May 2007; accepted 10 May 2007
Available online 31 May 2007

Abstract

The gas-phase hydride abstraction of methylamine with $Cu^+(^1S)$ is theoretically investigated by using density functional theory. Geometries for all the stationary points involved are fully optimized at both the B3LYP/6-311++G(d,p) and B3LYP/6-311++G(3df,2p) levels and the reaction is analyzed in terms of the topology of potential energy surface. Approach of Cu^+ towards methylamine could form either "classical" N or "nonclassical" η^1-methyl-H attached complex with the former being the global minimum. Both complexes are found to be key intermediates for the hydride abstraction, which could transfer into each other via two parallel routes, i.e., concerted metal movement and stepwise C–H activation-rearrangement. A charge-transfer process is detected for the "nonclassical" complex converting to a precursor species ($CuH–NH_2CH_2^+$), which accounts for the final products by a nonreactive dissociation.

Keywords: Hydride abstraction; Methylamine; Transition metal ion; Density functional theory; Atoms in molecules theory; Natural bond orbital theory

1. Introduction

Because of its unique importance in the global nitrogen cycle, biology processes, and organic syntheses [1–8], over the past two decades, the gas-phase reactivity of amines with metal ions has been investigated by a great body of studies, wherein hydride abstraction leading to metal hydride and hydride-abstracted amine ions is always a substantial, if not a major, reaction channel [9–16]. For instance, Radecki and Allison have reported that Co^+ abstracts a hydride unit from amines to form CoH whenever there is an α-hydrogen available but not when there is no α-hydrogen [10]. Armentrout et al. have experimentally studied the kinetic energy dependence of the endothermic hydride abstraction reactions of M^+ (M = V, Cr, and Ti) with methyl-substituted amines (methylamine, dimethylamine, and trimethylamine) and obtained the first experimental measurement of gas-phase bond dissociation energies for the corresponding transition metal hydrides [11,12]. Furthermore, rates for the hydride abstraction from methyl-substituted amines via reaction with Ag^+ and Cu^+ have been measured in all cases except for Ag^+ with methylamine in a flow reactor at ambient room temperature [13]. On the other hand, hydride abstraction has also been found to be an extensive reaction channel in the photodissociation of Mg^+–amine complexes [14–16].

Recently, we have theoretically investigated the hydride abstraction mechanism of Mg^+–amine complexes [16–18]. Our results suggest the reaction involves indeed a "classical" N attached complex rather than a "nonclassical" form (such as methyl- or CH_2-attachment) and shares a common reaction mechanism – C^α–H activation, H migration, charge-transfer (CT), and decomposition. The driving force for this process is dictated by the special stability of iminium cations, which arises from the lower ionization potentials of their precursors relative to that of their partner, metal hydrides (MgH) [16–18]. In spite of these investigations, the hydride abstraction by transition metal ions is still worthy of theoretical consideration, since different

* Corresponding author. Tel.: +86 546 8396319; fax: +86 546 8392123.
E-mail address: wyguo@hdpu.edu.cn (W. Guo).

0022-328X/$ - see front matter © 2007 Elsevier B.V. All rights reserved.
doi:10.1016/j.jorganchem.2007.05.030

electronic configurations of the metal ions could result in significantly different structures and energetics of species involved, which are of particular importance in understanding a reaction mechanism and in modeling dynamic parameters for a reaction using statistical theory as well.

In this article, we select the hydride abstraction from methylamine via reaction with Cu^+ as a model of our study. This reaction is a fast bimolecular reaction established by the measurement of the reaction rate (2.1×10^{-9} cm^3 s^{-1}) and based on the experimental results and their implications a qualitative reaction mechanism has already been discussed [13]. Our objective of this work is to bridge the gap between experiments and theories for this type of reaction. Thus, structures and energies for all the species involved are calculated and discussed in detail.

2. Computational methods

Theoretical treatment of the title reaction was performed by using B3LYP functional in conjunction with both the B3LYP/6-311++G(d,p) and B3LYP/6-311++G-(3df,2p) basis sets. This method has been found to be quite reliable as far as metal containing systems are concerned, especially when Cu^+ ions are under study [19–25]. Vibrational frequencies of all the optimized species were calculated at the same levels to identify the stationary points (minima or transition states) and to estimate the zero point energy (ZPE) corrections that are applied to all reported energies. Scaling factor for the ZPE is selected as 0.961 [26]. In order to confirm transition states and their connected minima, intrinsic reaction coordinate (IRC) calculations [27,28] were performed to follow the reaction pathways. All the calculations were performed with GAUSSIAN 03 program [29].

We also made use of theories of atoms in molecules (AIM) and natural bond orbital (NBO) to characterize interactions between different groups for some key species involved. These calculations were performed by using the program packages of AIM2000 [30] and NBO5.0 [31].

3. Results and discussion

Geometries as well as structural parameters optimized at the B3LYP/6-311++G(d,p) and B3LYP/6-311++G-(3df,2p) levels of theory are shown in Fig. 1 for the reactants, intermediates, and products involved in the title reaction. Total energies (E) for these calculated species are reported in Table 1 together with zero point energies (ZPE), $\langle S^2 \rangle$, and natural atomic charges. The resulting potential energy surface (PES) is sketched in Fig. 2. From Table 1, we can find that the $\langle S^2 \rangle$ deviation for all the species is negligible, suggesting that spin contamination is negligibly small in all of the calculations. It can also be seen from Figs. 1 and 2 that the two basis sets employed give almost same results, hence only the B3LYP/6-311++G-(3df,2p) results will be used in the discussion except where specially indicated.

Although only a "classical" Cu^+–N attachment was reported previously [22,23], here, we find two encounter isomers (**1** and **3**) for the Cu^+–methylamine association. Species **1** corresponds to the "classical" one (see Fig. 1), which is the global minimum that has been studied using several different methods [22,23]. Briefly, this structure favors electron transfer from the N lone pair into a metal 3d/4s mixing orbital as reflected by the natural charge at the metal center (see Table 1) as well as by the change in the C–N bond length upon the attachment, which follows the well-known bond activation reinforcement (BAR) rule if with respect to C the more electronegativity of N is considered [32]. Also, the 3d/4s mixing at Cu^+ moves electron density away from the Cu^+–N bond axis and thus reduces the repulsion with the N lone pair. Both the effects account for the strengthening of the bond formed. Correspondingly, the Cu^+–N binding energy is calculated to be 60.7 kcal mol^{-1}, in good agreement with that obtained at the B3LYP/6-311++G(2df,2p)//B3LYP/6-311G(d,p) level (59.8 kcal mol^{-1}) [22] and a little larger than that obtained at the CCSD(T)/6-311++G(2d,2p)//MP2/6-31G(d) level (55.9 kcal mol^{-1}) [23]. It is this rather strong Cu^+–methylamine association that explains the reaction of $Cu^+ + CH_3NH_2 \rightarrow CuH + CH_2NH_2^+$ as observed at thermal energy [13]. It is important to note that for the complex, in spite of the above-mentioned electron transfer, the positive charge is still centralized mainly on the metal center due to a back-donation of part of charge to the higher electronegative N atom from the metal [22].

Although not reported in the literatures for the ion-neutral association [22,23], we find a "nonclassical" η^1-methyl-H attached complex, species **3**, which is 30 kcal mol^{-1} less stable than **1** but lies still 30.7 kcal mol^{-1} lower in energy than the entrance channel. This new association is featured by a C_s symmetry with Cu^+–H^1–C–N as the symmetry plane favored by the H coordination trans with respect to the N lone pair. Note that the Cu^+–H–C structure is reminiscent of the so-called agostic interaction that was introduced by Brookhart and Green to describe the interaction of C–H bond with transition metals [33]. In fact, an inspection of Fig. 1 shows that in this adduct, the coordinated C–H bond is largely stretched (1.276 Å) and the Cu^+–H bond is also shortened to the regular range for the Cu^+–H–C agostic interaction [34]. Also, the molecular graph as depicted in Fig. 3 shows the value of ρ (0.078 e au^{-3}) at the Cu^+–H bond critical point (BCP) is almost the same as those found for the Cu^+–H–X (X = P, As, or C) agostic interaction in $H_3CCH_2XH_2$ (X = P and As)–Cu^+ complexes [34] and the $\nabla^2\rho$ value (0.151 e au^{-5}) at the BCP is also located in the range (0.15–0.25 e au^{-5}) for a typical agostic bond [35]. However, A more careful inspection of the graph shows that the bond path is indeed not curved near the hydrogen atom, as is always taken by agostic bonds [34,35]. Furthermore, a second-order NBO analysis has shown that the lengthening of the X–H bond, for the agostic interactions in ethylphosphine–Cu^+ and ethylarsine–Cu^+ complexes, arises from

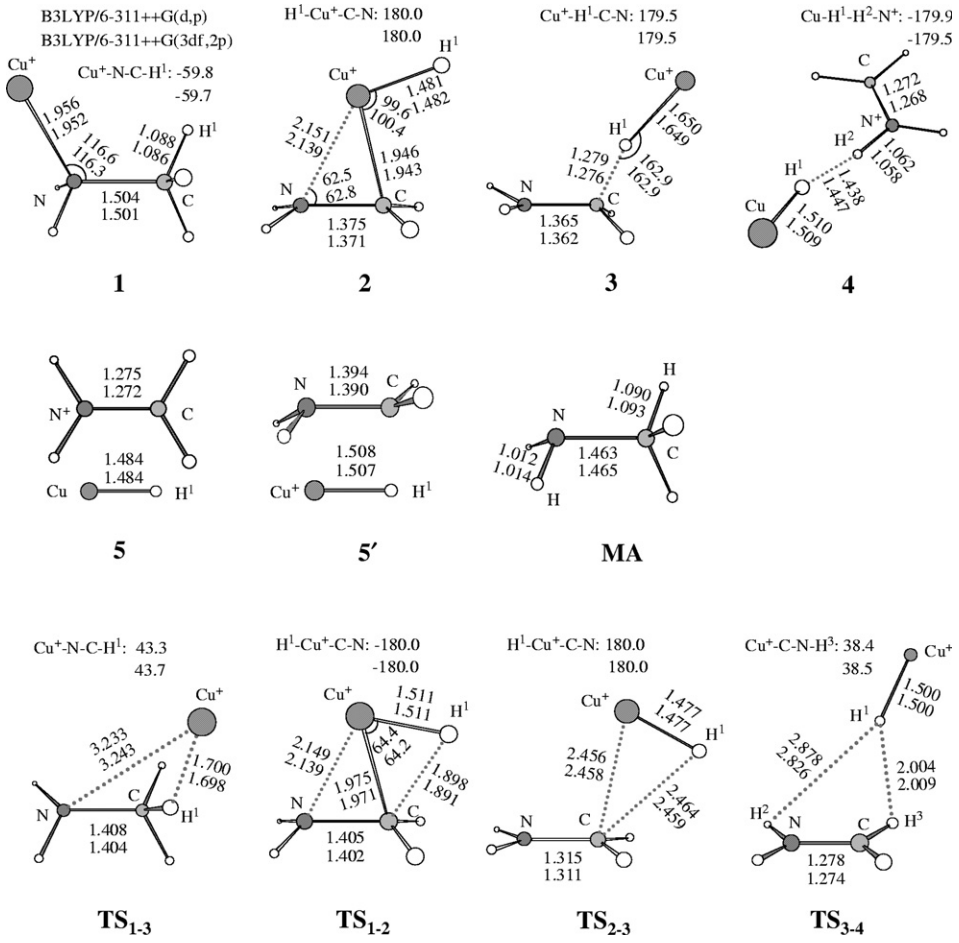

Fig. 1. Optimized structures for reactants, products, intermediate minima, and transition states involved in the hydride abstraction of CH_3NH_2 with Cu^+ at the B3LYP/6-311++G(d,p) and B3LYP/6-311++G(3df,2p) levels. Bond lengths are in angstroms and bond angles in degrees.

Table 1
Calculated total energies *E*s, zero point energies ZPEs (hartree), $\langle S^2 \rangle$, and natural atomic charges (e) for all the species involved in the hydride abstraction of methylamine with Cu^+

Spieces	B3LYP/6-311++G(d,p)			B3LYP/6-311++G(3df,2p)			Charges[a]
	E	ZPE	$\langle S^2 \rangle$	*E*	ZPE	$\langle S^2 \rangle$	
Cu^+	−1640.1769066	0.000000	0.000	−1640.1769066	0.000000	0.000	–
CH_3NH_2	−95.8938893	0.063786	0.000	−95.9003513	0.063758	0.000	–
CuH	−1641.0735373	0.004286	0.000	−1641.0739374	0.004247	0.000	–
$CH_2NH_2^+$	−95.0054038	0.054076	0.000	−95.0121992	0.054137	0.000	–
CuH^+	−1640.7220243	0.003773	0.755	−1640.7224139	0.003748	0.755	–
CH_2NH_2	−95.2377784	0.049875	0.754	−95.2441589	0.049825	0.754	–
1	−1736.1715314	0.067495	0.000	−1736.177564	0.067461	0.000	0.848
2	−1736.1002836	0.061639	0.000	−1736.1080029	0.061600	0.000	0.596
3	−1736.1176375	0.061935	0.000	−1736.1244178	0.061940	0.000	0.650
4	−1736.1075499	0.059164	0.000	−1736.1146776	0.059194	0.000	0.095
5($CuH + CH_2NH_2^+$)	−1736.0789411	0.058362	0.000 + 0.000	−1736.0861366	0.058384	0.000 + 0.000	0.000
5′ ($CuH^+ + CH_2NH_2$)	−1735.9598027	0.053648	0.755 + 0.754	−1735.9665728	0.053573	0.755 + 0.754	1.000
$\mathbf{TS}_{1-3}$	−1736.111044	0.062573	0.000	−1736.1180615	0.062566	0.000	0.868
$\mathbf{TS}_{1-2}$	−1736.0949299	0.060564	0.000	−1736.1022829	0.060547	0.000	0.841
$\mathbf{TS}_{2-3}$	−1736.0943058	0.060136	0.000	−1736.1016005	0.060142	0.000	0.351
$\mathbf{TS}_{3-4}$	−1736.0984272	0.059450	0.000	−1736.1059675	0.059539	0.000	0.039

[a] Values calculated at the NBO//B3LYP/6-311++G(d,p) level; values refer to charges located on Cu for **1** and $\mathbf{TS}_{1-3}$ while for the others on CuH.

the existence of donation from a σ(X–H) (X = C, P, or As) bonding orbital to a vacant 4s orbital of the metal and back-donation from a filled metal 3d orbital to a σ*(X–H) antibonding orbital of the bases [34]. In the case of species **3**, however, a different situation can be found from the NBO analysis (see Tables 2 and 3). In addition

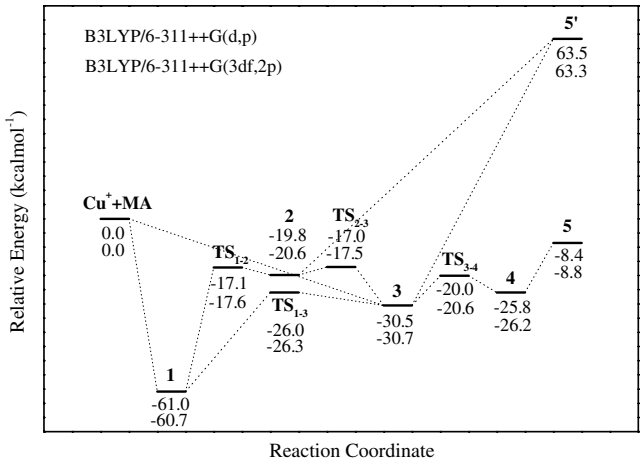

Fig. 2. Potential energy surface associated with the hydride abstraction of CH_3NH_2 with Cu^+ calculated at the B3LYP/6-311++G(d,p) and B3LYP/6-311++G(3df,2p) levels of theory. The scaling factor for ZPE is 0.961 [26].

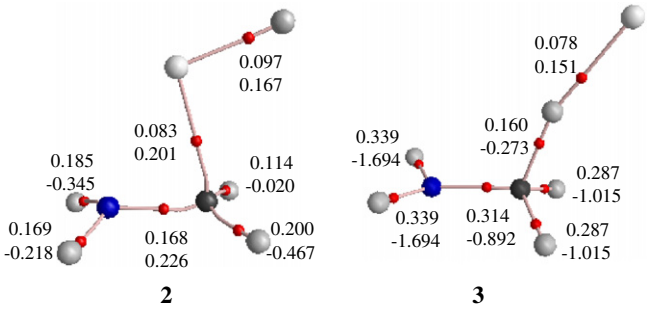

Fig. 3. Position of the bond critical points and bond paths from AIM theory for species **2** and **3**. For each critical point, the upper number corresponds to electron density, and the lower number corresponds to the value of $\nabla^2\rho(r_c)$. Electron densities are in e au^{-3} and the Laplacians in e au^{-5}.

to no change in bonding situations for the NH_2CH_3 entity, as shown in Table 2, the η^1-methyl-H attachment involves a new σ^*(Cu–N) antibonding orbital (occupancy: 1.811). The species is stabilized by the existence of a main donation of the filled σ^*(Cu–N) antibonding orbital to σ^*(C–H^1), a back-donation from σ(C–H^1) to the empty σ(Cu–N) bonding orbital, as well as a σ^*(Cu–N) to σ(Cu–N) electron transfer (see Table 3). It is these electron transfers that result in the large lengthening of the C–H^1 bond as well as the binding of Cu^+ to H^1.

From Fig. 1 we can find that for **3** the C–N bond length (1.362 Å) is quite close to that of free aminomethyl radical (1.390 Å) and the Cu^+–H^1 bond length (1.649 Å) is also closer to that of free Cu^+H rather than free CuH. Moreover, on the basis of the natural atomic charge analysis, the positive charge of this complex is evident to locate primarily on the CuH entity (0.650 e; see Table 1). All these evidences suggest that the conformation of the complex could be explained as CH_2NH_2–CuH^+ rather than $CH_2NH_2^+$–CuH.

Table 2
Orbitals responsible for charge distributions in the $[CuH + CH_2NH_2]^+$ species together with their characters[a]

Species	Bonding/antibonding orbitals	Relative contributions[b]	Occupancies[b]
2	σ(Cu–C)	58.21% Cu(4s3d$^{1.58}$) 41.79% C(2s2p$^{10.67}$)	1.759
	σ(Cu–H^1)	41.77% Cu(4s3d$^{0.69}$) 58.23% H(1s)	1.856
TS$_{2-3}$	σ(Cu–H^1)	29.28% Cu(4s) 70.72% H(1s)	1.772
	π(C–N)	26.91% C(2p) 73.09% N(2p)	1.991
3	σ*(Cu–N)	6.73% Cu(4s) 93.27% N(2p)	1.811
	σ(C–H^1)	45.04% C(2s2p$^{4.54}$) 54.96% H(1s)	1.884
TS$_{3-4}$	σ(Cu–H^1)	21.07% Cu(4s) 78.93% H(1s)	1.966
	π(C–N)	28.56% C(2p) 71.44% N(2p)	1.999
4	σ(Cu–H^1)	17.54% Cu(4s) 82.46% H(1s)	1.904
	π(C–N)	31.33% C(2p) 68.67% N(2p)	1.999

[a] Not included are the σ bonding orbitals possessed by all the species, i.e., one σ(C–N), two σ(C–H)'s, and two σ(N–H)'s in CH_2NH_2 or $CH_2NH_2^+$.
[b] Values at the NBO//B3LYP/6-311++G(d,p) level.

Table 3
Second-order perturbation theory analysis of the Fock matrix in the NBO basis for the $[CuH + CH_2NH_2]^+$ species

Species	Orbitals involved	Orbital interaction energy (kcal mol^{-1})[a]
2	σ(Cu–C) → σ*(Cu–H^1)	45.07
	LP(N) → σ*(Cu–C)	48.99
	σ(Cu–H^1) → σ*(Cu–C)	37.78
	σ*(Cu–C) → σ*(Cu–H^1)	25.91
	LP(N) → σ*(Cu–H^1)	16.00
TS$_{2-3}$	σ(Cu–H^1) → π*(C–N)	21.74
	3d(Cu) → π*(C–N)	8.81
	3s(Cu) → π*(N–C)	1.95
	π(C–N) → σ*(Cu–H^1)	1.08
3	σ*(Cu–N) → σ*(C–H^1)	47.45
	σ(Cu–N) → σ*(C–H^1)	5.06
	3s(Cu) → σ*(C–H^1)	6.61
	3d(Cu) → σ*(C–H^1)	2.91
	σ(C–H^1) → 5s5p(Cu)	3.17
	σ(C–H^1) → σ(Cu–N)	22.59
	σ*(C–N) → σ(Cu–N)	12.08
TS$_{3-4}$	σ(Cu–H^1) → π*(C–N)	1.16
	σ(Cu–H^1) → σ*(C–H^3)	1.73
4	σ(Cu–H^1) → σ*(N–H^2)	30.23
	σ(Cu–H^1) → σ*(Cu–H^1)	1.18
	σ(N–H^2) → σ*(Cu–H^1)	1.46

[a] Values calculated at the NBO//B3LYP/6-311++G(d,p) level.

Encounter complexes **1** and **3** could transfer into each other via two parallel routes. The first one involves a concerted process, in which Cu^+ moves directly from the NH_2 end to the CH_3 side. IRC calculations as shown in Fig. 4 verify this process is connected by transition state $\mathbf{TS}_{1-3}$, which lies at 34.4 kcal mol^{-1} above **1** or at 4.4 kcal mol^{-1} above **3** (see Fig. 2). As Fig. 1 shows, this transition state assumes a large structural similarity to **3** so that it is indeed "late" on the PES.

The second route for the $\mathbf{1} \rightarrow \mathbf{3}$ conversion involves a stepwise (two-step) process, i.e., a C–H activation step and subsequently a rearrangement one via transition states $\mathbf{TS}_{1-2}$ and $\mathbf{TS}_{2-3}$, respectively, both of which have been verified by IRC calculations (see Fig. 4). In the first step, insertion of the metal into one of the C–H bonds of methylamine that destabilizes the system by 40.1 kcal mol^{-1} could convert **1** into **2**. The new species is also featured by a C_s symmetry with the symmetry plane defined by H^1–Cu^+–C–N, where Cu^+ is located just above the C–N bond with comparable Cu^+–N and Cu^+–C distances (2.139 and 1.943 Å, respectively). Although the rather short Cu^+–N length, an examination of the molecular graph based on the AIM theory suggests that for the complex no any bond, because of nonexistence of a BCP, is formed between the two atoms (see Fig. 3), whereas the metal really forms bonds with both the C and H^1 atoms. The bond angle of C–Cu^+–H^1 is calculated to be 100.4°, suggesting the metal center is sd hybridized upon the formation of these bonds. Indeed, a NBO analysis detects that for this species Cu^+ binds both H^1 and C via sd (sd_{xy}) hybridized orbitals (where the *xy* plane lies on the symmetry plane with the *x* axis polarized approximately along the Cu^+–N line) and the structure is stabilized by interactions among these metal bonds (both bonding and antibonding) and a N lone pair (see Tables 2 and 3). Note that in this species the positive charge is also evident to locate primarily on the CuH entity (0.596 e; see Table 1).

Complexes **1** and **2** are connected by transition state $\mathbf{TS}_{1-2}$, which lies at 43.1 kcal mol^{-1} above **1** or at 3.0 kcal mol^{-1} above **2**. The geometry of this transition state is largely similar to that of **2**, suggesting it is indeed a late transition state. On the other hand, transition state $\mathbf{TS}_{2-3}$ (C_s) that lies at 17.5 kcal mol^{-1} below the entrance channel is verified to connect **2** and **3** (see Fig. 4). This possibility involves an intra-rotation of CuH^+ in the C_s symmetry plane. However, very long distances are detected for both Cu and H^1 to C in the transition state, so neither of them can form covalent bonds with C. Indeed, NBO analysis shows that in this case both σ(Cu–C) as in **2** and σ(C–H^1) as in **3** are broken while a new π(C–N) bonding orbital is formed (see Table 2). Accordingly, the C–N bond is shortened to be more close to that of free $CH_2NH_2^+$ (see Fig. 1). These facts indicate that the conformation of $\mathbf{TS}_{2-3}$ should be $CH_2NH_2^+$–CuH, according with the calculated natural charge on CuH (0.351 e; see Table 1). It is interesting to note that for both the connected minima (**2** and **3**), as discussed above, the positive charge locates primarily on the CuH entity. Thus, the conversion of $\mathbf{2} \rightarrow \mathbf{TS}_{2-3} \rightarrow \mathbf{3}$ indeed involves forward and back CT processes between CH_2NH_2 and CuH^+, which can be verified by the highest occupied molecular orbital (HOMO) diagrams as depicted in Fig. 4c. In **2** and **3**, we can find the orbital delocalizes evenly over the whole complexes, whereas for the transition state the orbital, thus electron density, localizes mainly on the CuH entity.

In summary, although two parallel pathways, i.e., the concerted metal movement and the stepwise C–H activation-rearrangement, could transfer complex **1** into **3**, the concerted process might be more possible since it is not only more simple but is lower in energy also. In the following, we will discuss the further reaction of **3**.

An extensive intra-rotation of the CH_2NH_2 entity that destabilizes the system by 4.5 kcal mol^{-1} could transfer **3** into **4**, a CT species. Structurally, this new species is strictly analogous to the CT species found in the hydride abstraction of Mg^+–NH_2CH_3 (**M2**; see [18]), i.e., an approximately planar structure with H^1 of the CuH entity attached to one H (H^2) of the N–H bonds favored by an nearly linear Cu–H^1–H^2–N association (C_s symmetry; see Fig. 1). The calculated C–N bond length is 1.268 Å, much close to that of free $CH_2NH_2^+$ (1.272 Å) and the natural charge of CuH is calculated to be only 0.095 e (see Table 1). All these facts make us believe that the conformation of this species could be explained as $CH_2NH_2^+$–HCu and the $\mathbf{3} \rightarrow \mathbf{4}$ conversation indeed involves a CT process between CH_2NH_2 and CuH^+. It is interesting to note that such a process has been extensively found in Mg^+–amine reactions [16–18], which may be driven by the ionization potential difference between iminium radical and magnesium hydride. For the Cu^+ + methylamine system, a similar situation is expected if the ionization potentials of CuH (~9.5 eV) [36] and CH_2NH_2 (~6.3 eV) [18,37] are considered. To gain a further insight into the interaction between $CH_2NH_2^+$ and CuH, NBO analysis is carried out for this species at the B3LYP/6-311++G(d,p) level. In the ground-state electronic configuration, the same bonding situations as in $\mathbf{TS}_{2-3}$ are found for **4** (see Table 2). As given in Table 3, The total donor–acceptor stabilization between CuH and $CH_2NH_2^+$ are calculated to be 32.9 kcal mol^{-1}, which is contributed mainly by the Cu–H^1 σ-bond donation into the σ*(N–H^2) antibonding orbital (30.2 kcal mol^{-1}).

The CT process involves $\mathbf{TS}_{3-4}$ (C_1), which has been confirmed carefully by IRC calculations (see Fig. 4d). This possibility involves an energy barrier of 10.1 kcal mol^{-1} with respect to **3**, which still lies at 20.6 kcal mol^{-1} below the entrance channel. The structure of the transition state is analogous to that of $\mathbf{TS}_{2-3}$, with the exception that CuH locates slantwise above $CH_2NH_2^+$. NBO analysis of the transition state as tabulated in Table 2 shows that its bonding situations are also the same as those in $\mathbf{TS}_{2-3}$ and **4** and the natural charge of CuH is only 0.039 e, the least one (see Table 1). These facts make us believe that the conformation of $\mathbf{TS}_{3-4}$ can also be explained as

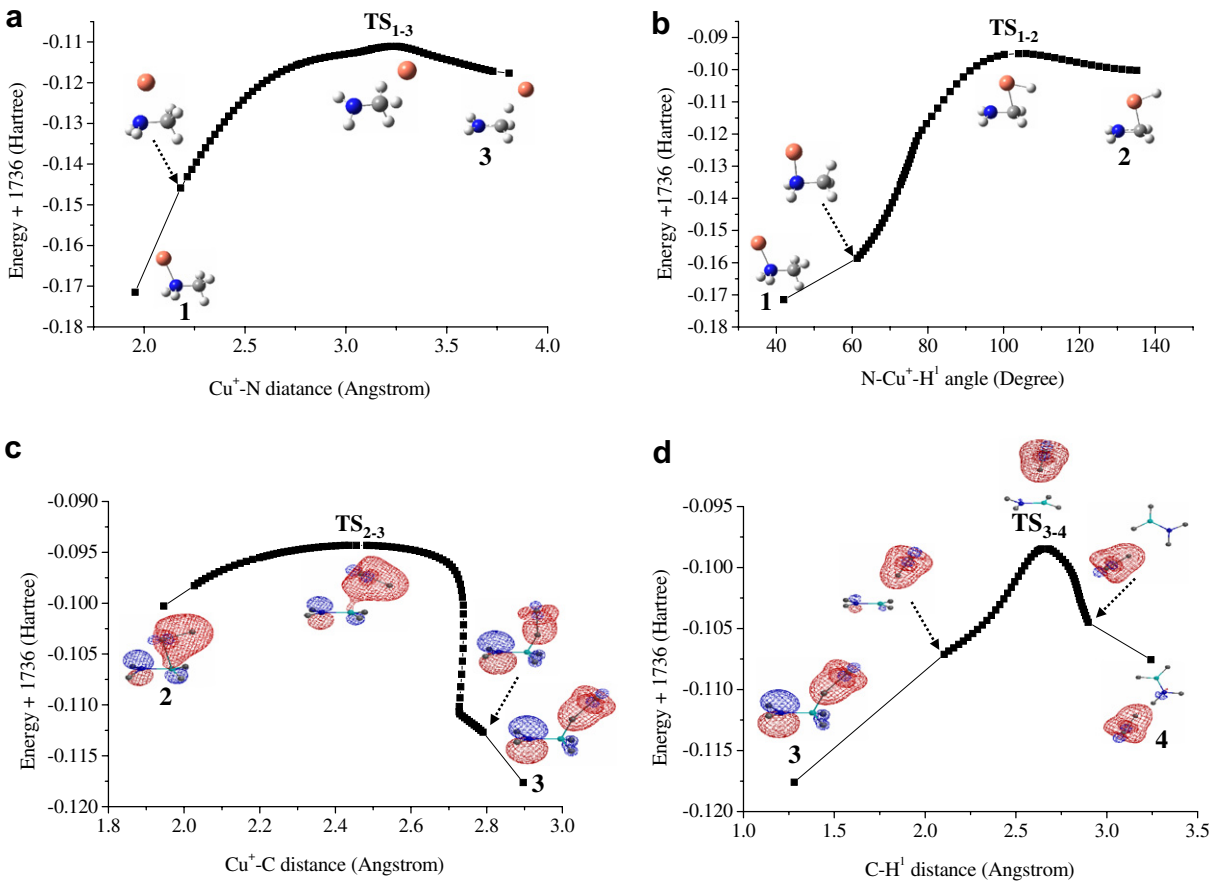

Fig. 4. Potential energy surface (PES) from IRC calculations for each step of the hydride abstraction of CH_3NH_2 with Cu^+ at the B3LYP/6-311++G(d,p) level. In (a) and (b), some selected structures are also included, while also included in (c) and (d) are highest occupied molecular orbitals (HOMO) for some selected species.

$CH_2NH_2^+$–HCu and the CT in the **3** → **4** process should take place "early", which is clearly mirrored by the HOMO features depicted in Fig. 4d.

It is important to give a general relation between charge distributions and geometries for $[CH_2NH_2–CuH]^+$ species. As shown in Table 2, for the $CH_2NH_2–CuH^+$ species, e.g., **2** and **3**, the carbon atom always forms covalent bonds with four atoms, i.e., a C–N and two C–H σ bonding orbitals in CH_2NH_2 and a σ bonding orbital with Cu (as in **2)** or H (as in **3)** from the CuH entity, through sp^3 hybridized orbitals. In this situation, because of the saturation effect of covalent bonds, the carbon atom cannot form further a π bonding orbital with N, thus hindering the system from forming $CH_2NH_2^+$. However, owing to the large distances between C and CuH (Cu and H), in the $CH_2NH_2^+$–CuH species (e.g., $\mathbf{TS}_{2–3}$, $\mathbf{TS}_{3–4}$, and **4**) the C atom cannot form the fourth covalent bond with any atom of the CuH entity but have to forms a π orbital with N. Meanwhile, the uncoupled electron of the CH_2NH_2 radical should move into CuH^+ giving these CT species due to the lower ionization potential of CH_2NH_2 with respect to CuH as mentioned above. It should be pointed out that the final values of charges on the CuH entity are also dictated by donor–acceptor interactions between the two constituents, which are determined by the structure of the species. For instance, in $\mathbf{TS}_{2–3}$ (C_s), the very location of CuH above $CH_2NH_2^+$ favors electron donation from σ(Cu–H^1) to π*(C–N) (see Table 3), thus on CuH more positive charge is found (see Table 1). Whereas for $\mathbf{TS}_{3–4}$ (C_1) the slantwise location of CuH above $CH_2NH_2^+$ does not favor electron transfers between the two entities (see Table 3), thus the charge located on CuH is nearly zero (see Table 1).

A nonreactive dissociation from **4** would account for the product of $CH_2NH_2^+ + CuH$ (**5**). The binding energy between CuH and $CH_2NH_2^+$ is calculated to be 17.4 kcal mol^{-1}, thus the overall reaction of $Cu^+ + CH_3NH_2 \rightarrow CH_2NH_2^+ + CuH$ is exothermic by 8.8 kcal mol^{-1}, according well with the expectation (6 kcal mol^{-1}) made according to thermochemical data [23].

An alternative hydride abstraction product arising from the $Cu^+ + CH_3NH_2$ reaction is $CH_2NH_2 + CuH^+$ (**5′**), which could be produced by a direct dissociation of the $CH_2NH_2–CuH^+$ bond of **2** and/or **3**. This product is calculated to be 72.2 kcal mol^{-1} higher in energy than its CT counterpart (**5**), in good agreement with the energy difference between **5′** and **5** (74 kcal mol^{-1}) estimated with the ionization potentials of CH_2NH_2 (~6.3 eV) [18,37] and CuH (~9.5 eV) [36]. It is this large energy difference that

dictates $CH_2NH_2^+ + CuH$ (**5**) rather than $CH_2NH_2 + CuH^+$ (**5′**) to be the product of Cu^+ reaction with CH_3NH_2 as observed in the experiment [13].

Sigsworth and Castleman have determined the rate of hydride abstraction to be 2.1×10^{-9} cm^3 s^{-1} for the reaction of methylamine with ground-state Cu^+, and assumed that the initial attack of the metal to the methylamine molecule occurs at the lone pair of nitrogen, which is followed by a H shift from C (or C–H activation) and a subsequent elimination of the neutral metal hydride [13]. The present theoretical calculations add new insight into the experimental findings. We also plan to survey PESs for hydride abstraction reactions of other transition metal ions with amines in order to find a general mechanistic profile. A more detailed description of these theoretical results will be presented in another separated paper.

4. Conclusions

The present theoretical calculations add new insight into the experimental findings for the hydride abstraction of methylamine with $Cu^+(^1S)$ in the gas phase. In addition to the "classical" N attached complex as realized earlier [22,23], copper cation is also found to η^1-attach to the hydrogen atom of CH_3 trans with respect to the N lone pair of methylamine to form a "nonclassical" complex. Both encounter complexes are found to be key intermediates for the hydride abstraction. The "classical" form is a global minimum but it could transfer into the less stable "nonclassical" one through two parallel routes, i.e., concerted metal movement and stepwise C–H activation-rearrangement. A subsequent charge-transfer step from the "nonclassical" complex results in a hydride abstraction precursor ($CuH–NH_2CH_2^+$) and a nonreactive dissociation of this new species would account for the hydride abstraction products. This charge-transfer process is favorable because the ionization potential of copper hydride is ~3.2 eV higher than that of aminomethyl radical and, for the $[CH_2NH_2–CuH]^+$ species involved, distributions of the positive charge are found to be strictly determined by their structures, i.e., the positive charge will localize primarily on the CuH entity when one atom of CuH could forms a σ covalent bond with the fourth sp^3 hybridized orbital at the carbon atom, otherwise, it should localize on CH_2NH_2.

Acknowledgements

This work was supported by SRF for ROCS, NCET-05-0608, Excellent Young Teachers Program, and Key Project (104119) of MOE, PR China, National Natural Science Foundation of China (20476061), and Natural Science Foundation of Shandong Province (Y2006B35).

References

[1] A. van Neste, R.A. Duce, C. Lee, Geophys. Res. Lett. 14 (1987) 711.
[2] D. Smith, B.J. Mclntosh, N.G. Adams, J. Chem. Phys. 90 (1989) 6213.
[3] G. Bouchoux, F. Djazi, M.T. Nguyen, J. Tortajada, J. Phys. Chem. 100 (1996) 3552.
[4] E.M. Cruz, J.E. Fowler, X. Lopez, J.M. Ugalde, J. Phys. Chem. A 101 (1997) 4807.
[5] D.R. Corbin, S. Schwarz, G.C. Sonnichsen, Catal. Today 37 (1997) 71.
[6] H.T. Deng, P. Kebarle, J. Phys. Chem. A 102 (1998) 571.
[7] S. Hoyau, K. Norrman, T.B. McMahon, G. Ohanessian, J. Am. Chem. Soc. 121 (1999) 8864.
[8] E.L. Øiestad, E. Uggerud, Int. J. Mass. Spectrom. 199 (2000) 91.
[9] S. Karrass, T. Priisse, K. Eller, H. Scbwarz, J. Am. Chem. Soc. 111 (1989) 9018.
[10] B.D. Radecki, J. Allison, J. Am. Chem. Soc. 106 (1984) 946.
[11] Y.-M. Chen, D.E. Clemmer, P.B. Armentrout, J. Chem. Phys. 95 (1991) 1228.
[12] Y.-M. Chen, D.E. Clemmer, P.B. Armentrout, J. Chem. Phys. 98 (1993) 4929.
[13] S.W. Sigsworth, J.A.W. Castleman, J. Am. Chem. Soc. 111 (1989) 3566.
[14] W.Y. Guo, H.C. Liu, S.H. Yang, J. Chem. Phys. 116 (2002) 2896.
[15] W.Y. Guo, H.C. Liu, S.H. Yang, J. Chem. Phys. 116 (2002) 9690.
[16] H.C. Liu, Y.H. Hu, S.H. Yang, W.Y. Guo, X.Q. Lu, L.M. Zhao, Chem. Eur. J. 11 (2005) 6392.
[17] W.Y. Guo, T. Yuan, X.F. Chen, L.M. Zhao, X.Q. Lu, S.J. Wu, J. Mol. Struc.-Theochem. 764 (2006) 177.
[18] W.Y. Guo, X.Q. Lu, S.Q. Hu, S.H. Yang, Chem. Phys. Lett. 381 (2003) 109.
[19] T. Zeigler, Chem. Rev. 91 (1991) 651.
[20] J.M. Seminario, Density Functional Theory: Advances in Quantum Chemistry, Academic Press, New York, 1998.
[21] J.F. Harison, Chem. Rev. 100 (2000) 679.
[22] A. Luna, B. Amekraz, J. Tortajada, Chem. Phys. Lett. 266 (1997) 31.
[23] S. Hoyau, G. Ohanessian, Chem. Phys. Lett. 280 (1997) 266.
[24] A. Luna, M. Alcamí, O. Mó, M. Yáñez, Int. J. Mass. Spectrom. 201 (2000) 215.
[25] A. Luna, M. Alcamí, O. Mó, M. Yáñez, Chem. Phys. Lett. 320 (2000) 129.
[26] L.M. Zhao, R.R. Zhang, W.Y. Guo, S.J. Wu, X.Q. Lu, Chem. Phys. Lett. 414 (2005) 28.
[27] C. Gonzalez, H.B. Schlegel, J. Chem. Phys. 90 (1989) 2154.
[28] C. Gonzalez, H.B. Schlegel, J. Phys. Chem. 94 (1990) 5523.
[29] M.J. Frisch, G.W. Trucks, H.B. Schlegel, G.E. Scuseria, M.A. Robb, J.R. Cheeseman, J.A. Montgomery Jr., T. Vreven, K.N. Kudin, J.C. Burant, J.M. Millam, S.S. Iyengar, J. Tomasi, V. Barone, B. Mennucci, M. Cossi, G. Scalmani, N. Rega, G.A. Petersson, H. Nakatsuji, M. Hada, M. Ehara, K. Toyota, R. Fukuda, J. Hasegawa, M. Ishida, T. Nakajima, Y. Honda, O. Kitao, H. Nakai, M. Klene, X. Li, J.E. Knox, H.P. Hratchian, J.B. Cross, C. Adamo, J. Jaramillo, R. Gomperts, R.E. Stratmann, O. Yazyev, A.J. Austin, R. Cammi, C. Pomelli, J.W. Ochterski, P.Y. Ayala, K. Morokuma, G.A. Voth, P. Salvador, J.J. Dannenberg, V.G. Zakrzewski, S. Dapprich, A.D. Daniels, M.C. Strain, O. Farkas, D.K. Malick, A.D. Rabuck, K. Raghavachari, J.B. Foresman, J.V. Ortiz, Q. Cui, A.G. Baboul, S. Clifford, J. Cioslowski, B.B. Stefanov, G. Liu, A. Liashenko, P. Piskorz, I. Komaromi, R.L. Martin, D.J. Fox, T. Keith, M.A. Al-Laham, C.Y. Peng, A. Nanayakkara, M. Challacombe, P.M.W. Gill, B. Johnson, W. Chen, M.W. Wong, C. Gonzalez, J.A. Pople, GAUSSIAN 03, Revision B.05, Gaussain Inc., Pittsburgh, PA, 2003.
[30] F. Biegler-König, J. Schönbohm, D. Bayles, AIM2000, University of Applied Science, Bielefeld, Germany, 2000.
[31] E.D. Glendening, J.K. Badenhoop, A.E. Reed, J.E. Carpenter, J.A. Bohmann, C.M. Morales, F. Weinhold, NBO5.0, Theoretical Chemistry Institute, University of Wisconsin, Madison, WI, 2001.
[32] M. Alcamí, O. Mó, M. Yáñez, Mass Spectrom. Rev. 20 (2001) 195.
[33] M. Brookhart, M.L.H. Green, J. Organomet. Chem. 250 (1983) 395.

[34] L. Galiano, M. Alcamí, O. Mó, M. Yáñez, J. Phys. Chem. A 106 (2002) 9306.
[35] P.L.A. Popelier, G. Logothetis, J. Organomet. Chem. 555 (1998) 101.
[36] M.C. Daza, G. Restrepo, E.A. Uribem, J.L. Villaveces, Chem. Phys. Lett. 428 (2006) 55.
[37] S.G. Lias, J.E. Bartmess, J.F. Liebman, J.L. Holmes, R.D. Levin, in: P.J. Linstrom, W.G. Mallard (Eds.), NIST Chemistry WebBook, NIST Standard Reference Database Number 69, Ion Energetics Data, National Institute of Standards and Technology, Gaithersburg MD, 20899, March 2003. <http://webbook.nist.gov>.